Nonlinear Layer Hall Effect and Detection of the Hidden Berry Curvature Dipole in $\mathcal{PT}$-Symmetric Antiferromagnetic Insulators

Zhuo-Hua Chen, Hou-Jian Duan, Ming-Xun Deng,* and Rui-Qiang Wang†

^{1}*Guangdong Basic Research Center of Excellence for Structure and Fundamental Interactions of Matter,*
Guangdong Provincial Key Laboratory of Quantum Engineering and Quantum Materials,
School of Physics, South China Normal University, Guangzhou 510006, China and
^{2}*Guangdong-Hong Kong Joint Laboratory of Quantum Matter,*
Frontier Research Institute for Physics, South China Normal University, Guangzhou 510006, China

Recent experimental and theoretical studies have revealed the emergence of a linear layer Hall effect (LHE) induced by hidden Berry curvature in MnBi$_2$Te$_4$ thin films. This phenomenon underscores the layer degree of freedom as a novel mechanism for generating Hall transport in layered materials, providing a new pathway to probe and manipulate the internal structure of fully compensated topological antiferromagnets (AFMs). In this work, we predict a nonlinear LHE in $\mathcal{PT}$-symmetric layered AFMs, which manifests as a detectable nonlinear Hall conductivity even with respect to the AFM order and odd with respect to the vertical electric field, in contrast to the linear LHE. Furthermore, we demonstrate that the nonlinear Hall currents induced by the hidden BCD and quantum metric dipole (QMD) obey distinct symmetries and flow in different directions. Our proposed nonlinear LHE establishes an experimentally advantageous framework for exclusively probing the hidden BCD quantum geometry.

Berry curvature (BC), which describes the geometry properties of Bloch bands, plays an essential role in the development of modern topological physics[1]. The BC can give rise to the Hall effect when time-reversal ($\mathcal{T}$) symmetry is globally broken. Nevertheless, Sodemann and Fu recently proposed that nonlinear Hall effect can occur under a second-order electric field even in $\mathcal{T}$-invariant materials[2], where breaking $\mathcal{T}$ symmetry is no longer necessary. Instead, inversion ($\mathcal{P}$) symmetry breaking is required. The underlying mechanism involves the dipole moment of the BC over the occupied states, known as the Berry curvature dipole (BCD). This innovative concept has garnered considerable attention[3–16] and the related nonlinear transport provides a powerful tool for probing topological physics in solids[17–24].

The BCD and the resulting nonlinear Hall effect were theoretically predicted in bilayer WTe$_2$[4] and later experimentally observed[5]. Around the same time, the BCD has also been detected experimentally in other materials, including two-dimensional (2D) MoS$_2$[6, 7] and WSe$_2$[14], bilayer graphene[12], Weyl semimetals[13], and various topological materials[25–27]. Even so, probing the BCD quantum geometry is still significantly constrained by stringent symmetry requirements[2]. For instance, in $\mathcal{P}$-symmetric Weyl semimetals, the contributions from paired Weyl nodes are the same in magnitude but opposite in sign, leading to cancellation when summed over all Weyl nodes[28]. Typically, additional material engineering, such as lattice strain or interlayer twisting[6–11], is required to generate a measurable BCD. As such, novel detection and manipulation schemes are highly desirable.

The recent discovery of 2D van der Waals antiferromagnets (AFMs), in which both $\mathcal{P}$ and $\mathcal{T}$ symmetries are broken but $\mathcal{PT}$ symmetry is preserved[29], provides a promising platform for exploring quantum-geometry-induced nonlinear effects. The $\mathcal{PT}$ symmetry of AFMs ensures the vanishing of global BC. However, in A-type layered AFMs, such as MnBi$_2$Te$_4$, local BC remains finite[30]. This local BC has equal magnitude but opposite signs in layers related by $\mathcal{PT}$ symmetry, a phenomenon referred to as hidden BC[30]. Although hidden, the local BC can still be detected through a novel effect called the layer Hall effect (LHE)[30–38], where electrons in $\mathcal{PT}$-symmetry-connected layers deflect in opposite directions. The linear LHE has been experimentally observed in MnBi$_2$Te$_4$[36], with a remarkable value reaching about $0.5e^2/h$. Based on the linear LHE, the Néel vector in centrosymmetric magnetoelectric AFMs has been successfully detected[39], and the layer Nernst and thermal Hall effects in 2D AFMs have also been proposed[40].

A natural question that arises is whether the BCD quantum geometry can be probed in the nonlinear counterpart of the LHE. In this work, we answer this question in the affirmative. We propose a nonlinear LHE in $\mathcal{PT}$-symmetric AFMs induced by hidden BCD. To date, most studies of the nonlinear Hall effect in $\mathcal{PT}$-symmetric AFMs have focused on another quantum geometry, i.e., the quantum metric dipole (QMD)[41–45]. While nonlinear responses have been experimentally measured in AFMs as probes for the QMD[44, 45], the BCD effect was overlooked due to the $\mathcal{PT}$ symmetry. Actually, although the $\mathcal{PT}$ symmetry of AFMs results in the absence of global BCD, a layer-locked hidden BCD exists, which has yet to be explored. It is particularly important to understand how to disentangle the BCD from QMD quantum geometries in experiments, for the fact that when a vertical electric field is applied, as commonly done in experiments[44, 45], the broken $\mathcal{PT}$ symmetry allows the hidden BCD signal to coexist with the QMD.
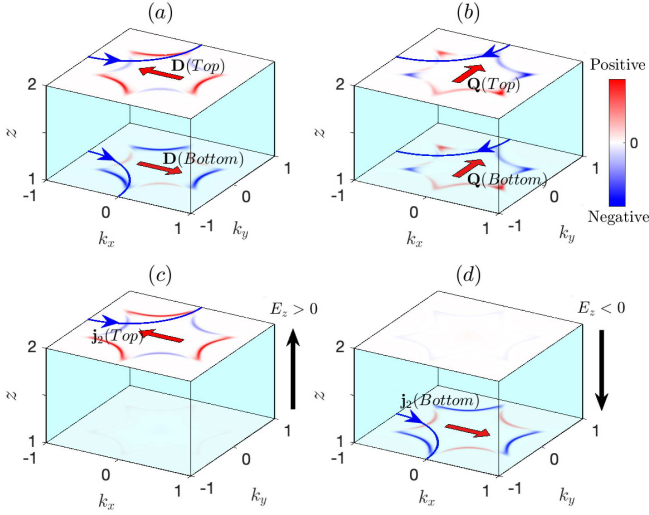
FIG. 1. Schematics of the (a) hidden-BCD-induced nonlinear LHE, (b) QMD-induced nonlinear anomalous Hall effect, and (c)-(d) BCD-induced layer-polarized nonlinear Hall currents in the presence of a vertical electric field E_z (black arrows). The blue and red filled hexagons indicate the distribution of the BC $\Omega_n^{xy}(\boldsymbol{k}, z)$ and quantum metric $\mathcal{R}_n^{yx}(\boldsymbol{k}, z)$ on the Fermi surfaces, with their dipoles $\boldsymbol{D}(z) = D_x^{xy}(z)\hat{x}$ and $\boldsymbol{Q}(z) = Q_y^{yx}(z)\hat{y}$ denoted by the red arrows inside the Fermi surfaces. The resulting nonlinear Hall currents $\boldsymbol{j}_2(z)$ are represented by the blue arrowed curves. In the nonlinear LHE, electrons on different layers are deflected spontaneously to opposite directions, due to the layer-locked BCD, while no such locking exists for the QMD.

We apply the nonlinear LHE to detect the hidden BCD unambiguously. The BCD and QMD can be conveniently distinguished through the nonlinear anomalous Hall conductivity, as, in certain directions, only one type of the nonlinear Hall effect survives, and their parities in the vertical electric field are opposite. Our findings not only expand the Hall effect family but also provide novel proposals for quantum geometry detection.

Symmetry analysis- The concept of hidden polarization has been proposed and applied to BC in several works [46–50]. A paradoxical duality is now recognized, where localized symmetry-breaking mechanism governs observable physical phenomena, despite the presence of a higher global symmetry that seemingly forbids such effects. Consider a $\mathcal{PT}$ symmetric layered AFM stacked along the z-direction. The layer-resolved BCD is defined as $\boldsymbol{D}(z) = \int d\boldsymbol{k} f_{\boldsymbol{k}} \partial_{\boldsymbol{k}} \Omega_{\boldsymbol{k}}(z)$, where $\Omega_{\boldsymbol{k}}(z)$ represents the BC in the z-layer, and $f_{\boldsymbol{k}}$ is the Fermi-Dirac distribution function. In A-type AFMs, each layer is a 2D ferromagnet. The $\mathcal{PT}$ symmetry requires $\Omega_{\boldsymbol{k}}(z) = \mathcal{PT}\Omega_{\boldsymbol{k}}(z)\mathcal{T}^{-1}\mathcal{P}^{-1} = -\Omega_{\boldsymbol{k}}(\bar{z})$, where $\bar{z} = \mathcal{P}z\mathcal{P}^{-1}$ is the inversion partner of z. The $\mathcal{PT}$-odd BC is fundamental to the linear LHE. Because $\mathcal{PT}\partial_{\boldsymbol{k}}\mathcal{T}^{-1}\mathcal{P}^{-1} = \partial_{\boldsymbol{k}}$ is $\mathcal{PT}$-even, the momentum-resolved BCD $\boldsymbol{D}(\boldsymbol{k}, z) = \partial_{\boldsymbol{k}}\Omega_{\boldsymbol{k}}(z)$ is $\mathcal{PT}$-odd, resulting in $\boldsymbol{D}(\boldsymbol{k}, z) = -\boldsymbol{D}(\boldsymbol{k}, \bar{z})$. Although

the global $\mathcal{PT}$ symmetry ensures that the net BCD vanishes, $\boldsymbol{D}(z)$ can exhibit a nonzero distribution across different layers, which is the so-called hidden BCD.

Naturally, upon the application of an electric field $\boldsymbol{E}$, the nonlinear Hall currents induced by the hidden BCD, $\boldsymbol{j}_2(z) = \frac{e^3\tau}{2}\hat{z} \times \boldsymbol{E}[\boldsymbol{D}(z) \cdot \boldsymbol{E}]$, as derived in Ref. [2], are equal in magnitude but opposite in sign for the z- and $\bar{z}$-layers. This implies that the electrons on the $\mathcal{PT}$-symmetry-related layers will deflect spontaneously in opposite directions, as depicted in Fig. 1(a). Since the LHE is contributed by nonlinear Hall currents, we dub it the nonlinear LHE. Note that nonlinear Hall effects can also arise from the nonlinear Drude and QMD mechanisms. However, both the Drude and QMD components are $\mathcal{PT}$-even and thus do not contribute to the nonlinear LHE, as illustrated in Fig. 1(b). Therefore, only the BCD mechanism needs to be considered when discussing the nonlinear LHE.

Theoretical model- Since $MnBi_2Te_4$ is extensively employed experimentally, we start from its low-energy effective Hamiltonian, whose nonmagnetic part reads [30–35]

$$\mathcal{H}(\boldsymbol{k}) = (\boldsymbol{d}_{\boldsymbol{k}} \cdot \boldsymbol{s})\sigma_x + M_{\boldsymbol{k}}\sigma_z + w(k_+^3 + k_-^3)\sigma_y, \quad (1)$$

where $\boldsymbol{d}_{\boldsymbol{k}} = (A_1 k_x, A_1 k_y, A_2 k_z)$, $k_{\pm} = k_x \pm ik_y$, $M_{\boldsymbol{k}} = M_0 - B_1 k_z^2 - B_2(k_x^2 + k_y^2)$, and $\boldsymbol{s}$ ($\boldsymbol{\sigma}$) represents the vector of the spin (orbit) Pauli matrices. Here, the $\mathcal{P}$ and $\mathcal{T}$ operators are given by $\mathcal{P} = \sigma_z$ and $\mathcal{T} = is_y\mathcal{K}$, respectively, with $\mathcal{K}$ being the complex conjugation operator. The model parameters can be found in Ref. [30]. The case with $M_0/B_1 > 0$ describes a 3D topological insulator, and the hexagonal warping term $\sim w$ reduces the full rotation symmetry down to C_{3z}. The A-type AFM order and the vertical electric field along the stacking z direction can be included through the tight-binding Hamiltonian

$$H = \sum_{z=1}^{n_z} c_z^\dagger [(h_0 + V_z)c_z + h_1 c_{z+1} + h_{-1}c_{z-1}], \quad (2)$$

with $V_z = (-1)^z m\boldsymbol{N} \cdot \boldsymbol{s} + eE_z[z - (n_z + 1)/2]$ and $h_n = \int dk_z \tilde{\mathcal{H}}(\boldsymbol{k})e^{ink_z}$. Here, $\boldsymbol{N} = (\sin\theta\cos\phi, \sin\theta\sin\phi, \cos\theta)$ represents the Néel vector of the AFM, and $\tilde{\mathcal{H}}(\boldsymbol{k})$ corresponds to Eq. (1) with the transformations $k_z \to \sin k_z$ and $k_z^2 \to 2 - 2\cos k_z$, as described in Refs. [51, 52].

The layer-resolved nonlinear conductivity induced by the BCD can be expressed as[53, 54]

$$\sigma_{\gamma;\alpha\beta}^{BCD}(z) = -\frac{e^3\tau}{\hbar^2}[D_\alpha^{\beta\gamma}(z) + D_\beta^{\alpha\gamma}(z)], \quad (3)$$

where $D_\alpha^{\beta\gamma}(z) = \sum_n \int d\boldsymbol{k} f_n \partial_{k_\alpha}\Omega_n^{\beta\gamma}(\boldsymbol{k}, z)$ is the α-th component of the BCD vector, and $f_n = 1/[e^{(\varepsilon_n - E_F)/k_B T} + 1]$ denotes the equilibrium distribution function. The layer-resolved BC corresponds to the imaginary part of the quantum geometric tensor[55]

$$\mathcal{Q}_{mn}^{\beta\gamma}(\boldsymbol{k}, z) = \frac{\langle m|v_\beta|n\rangle\langle n|v_\gamma(z)|m\rangle}{(\varepsilon_m - \varepsilon_n)^2}, \quad (4)$$
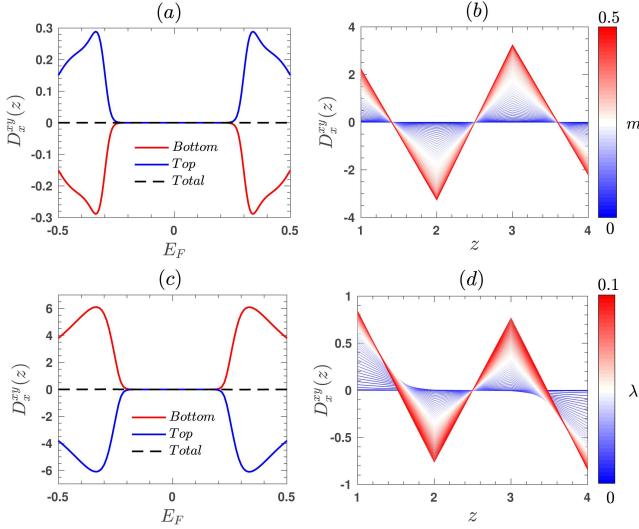
FIG. 2. Numerical results for the layer-resolved BCD induced by (a)-(b) the AFM order with $m = 0.5$, and (c)-(d) the tilt with $\lambda = 0.1$, where $n_z = 2$ and $n_z = 4$ are chosen in the left and right panels, respectively. The rest parameters for the calculations are taken as $\theta = 0$, $\phi = 0$, $w = 0.5$, $M_0 = 0.1$, $A_1 = A_2 = 0.55$, $B_1 = B_2 = 0.25$, and $E_z = 0$.

namely, $\Omega_n^{\beta\gamma}(\boldsymbol{k}, z) = \sum_{m \neq n} 2\,\mathrm{Im}[\mathcal{Q}_{mn}^{\beta\gamma}(\boldsymbol{k}, z)]$. Here, $|n\rangle$ is wavefunction for the energy ε_n of Eq. (2), $v_\beta = \partial_{k_\beta} \mathcal{H}(\boldsymbol{k})$ and $v_\gamma(z) = \hat{P}_z v_\gamma \hat{P}_z$, in which $\hat{P}_z$ denotes the projection operator constructed by the wavefunction on the z-layer [56–58]. From Eq. (4), we can define the layer-resolved band-normalized quantum metric $\mathcal{R}_n^{\beta\gamma}(\boldsymbol{k}, z) = \sum_{m \neq n} \mathrm{Re}[\mathcal{Q}_{mn}^{\beta\gamma}(\boldsymbol{k}, z)/(\varepsilon_m - \varepsilon_n)]$. The layer-resolved QMD-induced nonlinear conductivity takes the form[53, 54]

$$\sigma_{\gamma;\alpha\beta}^{QMD}(z) = -\frac{e^3}{\hbar}\{2Q_\gamma^{\alpha\beta}(z) - \frac{1}{2}[Q_\alpha^{\beta\gamma}(z) + Q_\beta^{\alpha\gamma}(z)]\}, \quad (5)$$

with $Q_\alpha^{\beta\gamma}(z) = \sum_n \int d\boldsymbol{k} f_n \partial_{k_\alpha} \mathcal{R}_n^{\beta\gamma}(\boldsymbol{k}, z)$. The $\mathcal{PT}$ symmetry ensures

$$\mathcal{Q}_{mn}^{\beta\gamma}(\boldsymbol{k}, z) = \mathcal{PT}\mathcal{Q}_{mn}^{\beta\gamma}(\boldsymbol{k}, z)\mathcal{T}^{-1}\mathcal{P}^{-1} = [\mathcal{Q}_{mn}^{\beta\gamma}(\boldsymbol{k}, \bar{z})]^*, \quad (6)$$

such that

$$\mathcal{R}_n^{\beta\gamma}(\boldsymbol{k}, z) = \mathcal{R}_n^{\beta\gamma}(\boldsymbol{k}, \bar{z}), \; \Omega_n^{\beta\gamma}(\boldsymbol{k}, z) = -\Omega_n^{\beta\gamma}(\boldsymbol{k}, \bar{z}). \quad (7)$$

Consequently, the $\mathcal{PT}$-odd hidden BCD contributes to the nonlinear LHE, while the $\mathcal{PT}$-even QMD makes no contribution.

In the AFM MnBi$_2$Te$_4$, the $\mathcal{PT}$-symmetric staggered magnetization breaks the interlayer $\mathcal{P}$ symmetry and intralayer $\mathcal{T}$ symmetry, leading to $\Omega_n^{\beta\gamma}(\boldsymbol{k}, z) = -\Omega_n^{\beta\gamma}(-\boldsymbol{k}, \bar{z})$ and $\Omega_n^{\beta\gamma}(\boldsymbol{k}, z) = \Omega_n^{\beta\gamma}(-\boldsymbol{k}, z)$ when $w = 0$. As a result, the BC with only out-of-plane component behaves as a pseudoscalar globally and the BCD in each layer behaves as a pseudovector. For $m = 0$, the warping term with both $\mathcal{P}$ and $\mathcal{T}$ symmetries can also induce a

BC that fulfills $\Omega_n^{\beta\gamma}(\boldsymbol{k}, z) = \Omega_n^{\beta\gamma}(-\boldsymbol{k}, \bar{z})$ and $\Omega_n^{\beta\gamma}(\boldsymbol{k}, z) = -\Omega_n^{\beta\gamma}(-\boldsymbol{k}, z)$. Consequently, when both m and w are finite, the parity of the BC with respect to $\boldsymbol{k}$ is broken. Nevertheless, the C_{3z} symmetry with a mirror line along the x-axis ensures $\mathcal{M}_y \Omega_n^{\beta\gamma}(\boldsymbol{k}, z)\mathcal{M}_y^{-1} = \Omega_n^{\beta\gamma}(\boldsymbol{k}, z)$ with $\mathcal{M}_y k_y \mathcal{M}_y^{-1} = -k_y$, as seen from Fig. 1(a). Therefore, $\mathcal{M}_y \partial_{k_y} \Omega_n^{\beta\gamma}(\boldsymbol{k}, z)\mathcal{M}_y^{-1} = -\partial_{k_y}\Omega_n^{\beta\gamma}(\boldsymbol{k}, z)$, making $D_y^{\beta\gamma}(z)$ vanish. The combined effects of the staggered magnetization and warping term give rise to a nonzero layer-locked BCD $D_x^{\beta\gamma}(z)$. Since $\boldsymbol{j}_2(z) \propto \hat{z} \times \boldsymbol{E}[\boldsymbol{D}(z) \cdot \boldsymbol{E}]$, the nonlinear LHE arises when the electric field is exerted along the x direction, with the layer Hall current orthogonal to the BCD vector $\boldsymbol{D}(z) = D_x^{xy}(z)\hat{x}$.

Numerical results- Firstly, we discuss the simplest case with the Néel vector along the z-direction. The layer-resolved BCD as a function of the Fermi energy E_F is plotted in Fig. 2(a). Obviously, for a bilayer structure, $D_x^{xy}(Top) = -D_x^{xy}(Bottom)$ is guaranteed by the global $\mathcal{PT}$ symmetry. For structures with more layers, the $\mathcal{PT}$ symmetric AFM pattern is always preserved, as illustrated in Fig. 2(b), where $D_x^{xy}(z) = -D_x^{xy}(\bar{z})$ with $\bar{z} = n_z + 1 - z$. This implies that the nonlinear Hall conductivities from $\mathcal{PT}$ partners are exactly compensated, thereby establishing the nonlinear LHE induced by the hidden BCD. In contrast to the linear LHE, which originates from m-odd BC, the nonlinear LHE is governed by m-even BCD, as shown in Fig. 3(a). Accordingly, in the nonlinear LHE, it is the breaking of $\mathcal{P}$-symmetry, rather than $\mathcal{T}$-symmetry, that plays a crucial role. To substantiate this, we replace the magnetization $m\boldsymbol{N} \cdot \boldsymbol{s}$ with a tilt λk_x and plot the BCD in Figs. 2(c) and (d). As expected, the scenario is reproduced similar to Figs. 2(a) and (b). This suggests that the proposed nonlinear LHE can also be realized in more nonmagnetic layered materials.

In Fig. 3, we plot the nonlinear layer Hall conductivity $\sigma_{y;xx}^{BCD}(Top) = -\sigma_{y;xx}^{BCD}(Bottom)$ as functions of the AFM order and warping parameters. In the phase of topological AFM insulator with $M_0/B_1 > 0$, $\sigma_{y;xx}^{BCD}(z)$ can be more than one order of magnitude greater than that in the trivial insulator with $M_0/B_1 < 0$, as observed in Fig. 3(a). The significant enhancement of $\sigma_{y;xx}^{BCD}(z)$ is attributed to the topological surface states, as shown in Fig. 3(b), where the surface states within the bulk band gap become decoupled and observable for $n_z > 20$. Different from the linear LHE[30–38], the nonlinear LHE requires the warping term to lower the full rotation symmetry in each layer. Specifically, the interplay of the warping term and AFM order breaks the symmetry of $D_x^{xy}(\boldsymbol{k}, z)$ in k_x, ensuring the nonzero result of $\sigma_{y;xx}^{BCD}(z)$. As the warping parameter w increases, the nonlinear LHE becomes more pronounced, as indicated in Fig. 3(c). Moreover, the nonlinear LHE can be further enhanced by tuning the Néel vector from out-of-plane to in-plane, as shown in Fig. 3(d).

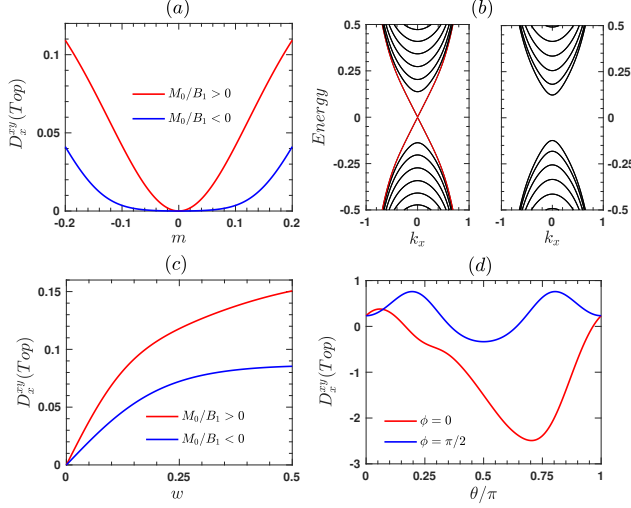As discussed above, due to the $\mathcal{PT}$ symmetry, the

FIG. 3. (a) The layer-resolved nonlinear Hall conductivity $\sigma_{y;xx}^{BCD}(Top) = -\sigma_{y;xx}^{BCD}(Bottom)$ as a function of m, with $\boldsymbol{N} = (0,0,1)$, $|M_0/B_1| = 0.4$, and $n_z = 2$. (b) The energy band for $m = 0$ and $n_z = 20$, with $M_0/B_1 < 0$ (right) and $M_0/B_1 > 0$ (left), where topological surface states emerge in the bulk band gap in the phase of topological AFM insulator. (c)-(d) $\sigma_{y;xx}^{BCD}(Top)$ as a function of w and the direction of the Néel vector, respectively. The rest parameters are the same as in Fig. 2(a).
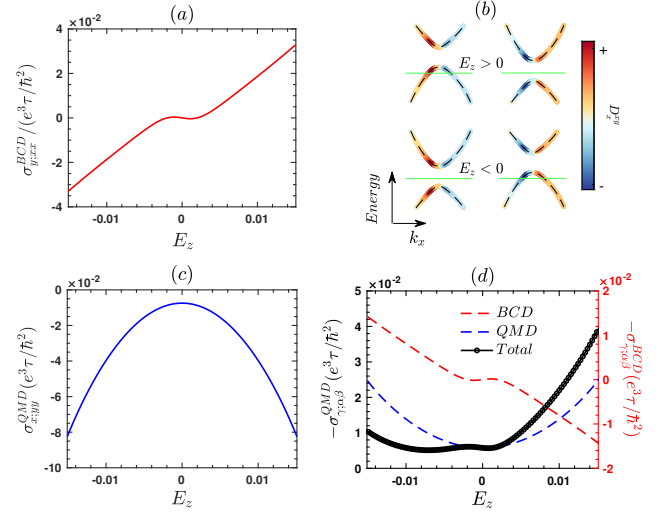

FIG. 4. (a) The net nonlinear Hall conductivity $\sigma_{y;xx}^{BCD}$ as a function of the vertical electric field. (b) The underlying physics of the hidden-BCD-induced nonlinear Hall conductivity, where the vertical electric field induces a potential difference between the top and bottom surfaces, leading to an imbalance of their Hall conductivity, as a result of the uncompensated hidden BCD of different layers when the global $\mathcal{PT}$ symmetry is broken. (c) The E_z-dependence of the QMD component $\sigma_{x;yy}^{QMD}$ and (d) the nonlinear Hall conductivities when the driving electric field is misaligned from the crystal axis.

BCDs on the z- and $\bar{z}$-layers are compensated, resulting in a vanishing net nonlinear Hall conductivity. In order to observe the nonlinear LHE, the $\mathcal{PT}$ symmetry must be broken, e.g., by applying a vertical electric field as illustrated in Figs. 1(c) and (d). Indeed, as shown in Fig. 4(a), a net anomalous nonlinear Hall conductivity emerges for finite E_z. Importantly, the nonlinear Hall signal flips sign when reversing E_z. This electric-field-reversible nonlinear Hall effect represents a fundamental piece of evidence for the nonlinear LHE. Physically, this behavior can be understood as follows. As E_z increases, the $\mathcal{PT}$ symmetry is progressively disrupted, causing the degenerate bands to split, see Fig. 4(b). Therefore, the BCD, in bilayer MnBi$_2$Te$_4$ for example, is dominated by the top/bottom layer, when the Fermi level crosses the band from the top/bottom layer. As a result, the BCDs on the z- and $\bar{z}$-layers are no longer compensated, leading to a detectable nonlinear anomalous Hall conductivity.

Notice that recent experiments have also investigated the application of an out-of-plane electric field in 2D materials, which can induce an electrically switchable BCD[5, 59–61]. In those works, the electric field is used to tune the band gap, driving a topological phase transition from a quantum spin Hall state to a normal insulating state, thereby enhancing the BCD near the topological critical points. The underlying physics of the nonlinear LHE proposed here is fundamentally different. In our case, the vertical electric field is adopted to lift the degeneracy imposed by $\mathcal{PT}$ symmetry, which provides an alternative pathway to detect or manipulate the BCD and its associated nonlinear response.

Comparison of BCD and QMD contributions-In $\mathcal{PT}$ symmetric AFMs, the nonlinear Hall effect can also be induced by the QMD[41–45]. However, the contribution from the QMD has the same sign across different layers, thus not contributing to the nonlinear LHE. To demonstrate this, we estimate the QMD contribution through Eq. (5), and verify that for the Hamiltonian of MnBi$_2$Te$_4$, as given in Eq. (2), $\sigma_{\gamma;\alpha\beta}^{QMD}$ vanishes whenever there is an odd number of y-subscripts, since the integral kernel in $Q_\alpha^{\beta\gamma}(z)$ is an odd function of k_y. As a consequence, only $\sigma_{x;yy}^{QMD}$ survives in the nonlinear anomalous Hall conductivity. In contrast, the dominated BCD contribution is $\sigma_{y;xx}^{BCD}$. Physically, the $\mathcal{M}_y$-odd symmetry of $\mathcal{R}_n^{\beta\gamma}(\boldsymbol{k}, z)$, i.e., $\mathcal{M}_y \mathcal{R}_n^{\beta\gamma}(\boldsymbol{k}, z) \mathcal{M}_y^{-1} = -\mathcal{R}_n^{\beta\gamma}(\boldsymbol{k}, z)$, different from the $\mathcal{M}_y$-even BC, causes the two nonlinear Hall currents to be perpendicular, as shown in Figs. 1(a) and (b). Thus, when the driving field is along a particular crystal axis, e.g., x- or y- axis, only one type of nonlinear Hall current survives, making it straightforward to distinguish between the BCD and QMD contributions.

Except for the direction-locked property, the BCD and QMD contributions can also be distinguished by their different dependences on the vertical electric field. As shown in Fig. 4(a), $\sigma_{y;xx}^{BCD}$ exhibits antisymmetry with respect to E_z due to the nonlinear LHE, while $\sigma_{x;yy}^{QMD}$ is

symmetric. Furthermore, $\sigma_{x;yy}^{QMD}$ can be finite even in the absence of E_z, as illustrated in Fig. 4(c), indicating that the QMD mechanism for the nonlinear Hall effect does not require the breaking of $\mathcal{PT}$ symmetry. When the driving electric field is misaligned from the crystal axis, the coexistence of both mechanisms leads to an asymmetric lineshape, as shown in Fig. 4(d). In this situation, one can isolate the symmetric component as the QMD contribution and the antisymmetric component as the BCD contribution. Notably, recent experiments on even-layer $MnBi_2Te_4$ have shown that the measured nonlinear Hall conductivity exhibits an asymmetric dependence on E_z, see Fig. 4(b) of Ref. [44] and Fig. 3(d) of Ref. [45].

Conclusion-In summary, we have proposed a nonlinear LHE induced by the hidden BCD in $\mathcal{PT}$-symmetric topological AFM insulators. The resulting nonlinear Hall conductivity exhibits a unique direction-locked property and a distinctive dependence on the modulation of the vertical electric field, contrasting with the QMD contribution. This nonlinear LHE provides an experimentally advantageous framework for probing the hidden BCD quantum geometry, even when it coexists with the QMD contribution. Moreover, the hidden-BCD-induced nonlinear LHE, which is sensitive to the orientation of the Néel vector, offers a means for the Néel vector detection in magnetoelectric AFMs with both in-plane and out-of-plane Néel vectors. Our results not only expand the Hall effect family but also extend the BCD physics to a broad range of material platforms with high tunability, offering promising prospects for practical applications.

* dengmingxun@scnu.edu.cn
† wangruiqiang@m.scnu.edu.cn

[1] D. Xiao, M.-C. Chang, and Q. Niu, Berry phase effects on electronic properties, Rev. Mod. Phys. **82**, 1959 (2010).

[2] I. Sodemann and L. Fu, Quantum nonlinear hall effect induced by berry curvature dipole in time-reversal invariant materials, Phys. Rev. Lett. **115**, 216806 (2015).

[3] Y. Zhang, Y. Sun, and B. Yan, Berry curvature dipole in weyl semimetal materials: An ab initio study, Phys. Rev. B **97**, 041101 (2018).

[4] Z. Z. Du, C. M. Wang, H.-Z. Lu, and X. C. Xie, Band signatures for strong nonlinear hall effect in bilayer wte$_2$, Phys. Rev. Lett. **121**, 266601 (2018).

[5] S.-Y. Xu, Q. Ma, H. Shen, V. Fatemi, S. Wu, T.-R. Chang, G. Chang, A. M. M. Valdivia, C.-K. Chan, Q. D. Gibson, J. Zhou, Z. Liu, K. Watanabe, T. Taniguchi, H. Lin, R. J. Cava, L. Fu, N. Gedik, and P. Jarillo-Herrero, Electrically switchable berry curvature dipole in the monolayer topological insulator wte2, Nature Physics **14**, 900 (2018).

[6] J. Son, K.-H. Kim, Y. H. Ahn, H.-W. Lee, and J. Lee, Strain engineering of the berry curvature dipole and valley magnetization in monolayer mos$_2$, Phys. Rev. Lett. **123**, 036806 (2019).

[7] J. Lee, Z. Wang, H. Xie, K. F. Mak, and J. Shan, Valley magnetoelectricity in single-layer mos2, Nature Materials **16**, 887 (2017).

[8] Z. He and H. Weng, Giant nonlinear hall effect in twisted bilayer wte2, npj Quantum Materials **6**, 101 (2021).

[9] S. Duan, F. Qin, P. Chen, X. Yang, C. Qiu, J. Huang, G. Liu, Z. Li, X. Bi, F. Meng, X. Xi, J. Yao, T. Ideue, B. Lian, Y. Iwasa, and H. Yuan, Berry curvature dipole generation and helicity-to-spin conversion at symmetry-mismatched heterointerfaces, Nature Nanotechnology **18**, 867 (2023).

[10] S. Sinha, P. C. Adak, A. Chakraborty, K. Das, K. Debnath, L. D. V. Sangani, K. Watanabe, T. Taniguchi, U. V. Waghmare, A. Agarwal, and M. M. Deshmukh, Berry curvature dipole senses topological transition in a moirésuperlattice, Nature Physics **18**, 765 (2022).

[11] M. Huang, Z. Wu, X. Zhang, X. Feng, Z. Zhou, S. Wang, Y. Chen, C. Cheng, K. Sun, Z. Y. Meng, and N. Wang, Intrinsic nonlinear hall effect and gate-switchable berry curvature sliding in twisted bilayer graphene, Phys. Rev. Lett. **131**, 066301 (2023).

[12] S.-C. Ho, C.-H. Chang, Y.-C. Hsieh, S.-T. Lo, B. Huang, T.-H.-Y. Vu, C. Ortix, and T.-M. Chen, Hall effects in artificially corrugated bilayer graphene without breaking time-reversal symmetry, Nature Electronics **4**, 116 (2021).

[13] D. Kumar, C.-H. Hsu, R. Sharma, T.-R. Chang, P. Yu, J. Wang, G. Eda, G. Liang, and H. Yang, Room-temperature nonlinear hall effect and wireless radiofrequency rectification in weyl semimetal tairte4, Nature Nanotechnology **16**, 421 (2021).

[14] M. Huang, Z. Wu, J. Hu, X. Cai, E. Li, L. An, X. Feng, Z. Ye, N. Lin, K. T. Law, and N. Wang, Giant nonlinear hall effect in twisted bilayer wse2, National Science Review **10**, nwac232 (2022).

[15] P. He, G. K. W. Koon, H. Isobe, J. Y. Tan, J. Hu, A. H. C. Neto, L. Fu, and H. Yang, Graphene moirésuperlattices with giant quantum nonlinearity of chiral bloch electrons, Nature Nanotechnology **17**, 378 (2022).

[16] K. Kang, T. Li, E. Sohn, J. Shan, and K. F. Mak, Nonlinear anomalous hall effect in few-layer wte2, Nature Materials **18**, 324 (2019).

[17] K. Yasuda, T. Morimoto, R. Yoshimi, M. Mogi, A. Tsukazaki, M. Kawamura, K. S. Takahashi, M. Kawasaki, N. Nagaosa, and Y. Tokura, Large non-reciprocal charge transport mediated by quantum anomalous hall edge states, Nature Nanotechnology **15**, 831 (2020).

[18] W. Zhao, Z. Fei, T. Song, H. K. Choi, T. Palomaki, B. Sun, P. Malinowski, M. A. McGuire, J.-H. Chu, X. Xu, and D. H. Cobden, Magnetic proximity and nonreciprocal current switching in a monolayer wte2 helical edge, Nature Materials **19**, 503 (2020).

[19] H. Isobe, S.-Y. Xu, and L. Fu, High-frequency rectification via chiral bloch electrons, Science Advances **6**,

eaay2497 (2020).

[20] H. Li, C. Zhang, C. Zhou, C. Ma, X. Lei, Z. Jin, H. He, B. Li, K. T. Law, and J. Wang, Quantum geometry quadrupole-induced third-order nonlinear transport in antiferromagnetic topological insulator mnbi2te4, Nature Communications 15, 7779 (2024).

[21] Z. Zhang, N. Wang, N. Cao, A. Wang, X. Zhou, K. Watanabe, T. Taniguchi, B. Yan, and W.-b. Gao, Controlled large non-reciprocal charge transport in an intrinsic magnetic topological insulator mnbi2te4, Nature Communications 13, 6191 (2022).

[22] S. Wang, X. Li, H. Zhang, B. Chen, H. Xie, C. Li, F. Fei, S. Zhang, and F. Song, Nonlinear hall effect and scaling law in sb-doped topological insulator mnbi4te7, Applied Physics Letters 124, 153102 (2024).

[23] Y. Fan, H. Wang, P. Tang, S. Murakami, X. Wan, H. Zhang, and D. Xing, Symmetry-driven anisotropic coupling effect in antiferromagnetic topological insulator: Mechanism for a quantum anomalous hall state with a high chern number, Phys. Rev. B 110, 035139 (2024).

[24] P. Bhalla, K. Das, D. Culcer, and A. Agarwal, Resonant second-harmonic generation as a probe of quantum geometry, Phys. Rev. Lett. 129, 227401 (2022).

[25] P. He, H. Isobe, D. Zhu, C.-H. Hsu, L. Fu, and H. Yang, Quantum frequency doubling in the topological insulator bi2se3, Nature Communications 12, 698 (2021).

[26] S. Dzsaber, X. Yan, M. Taupin, G. Eguchi, A. Prokofiev, T. Shiroka, P. Blaha, O. Rubel, S. E. Grefe, H.-H. Lai, Q. Si, and S. Paschen, Giant spontaneous hall effect in a nonmagnetic weyl–kondo semimetal, Proceedings of the National Academy of Sciences 118, e2013386118 (2021).

[27] A. Tiwari, F. Chen, S. Zhong, E. Drueke, J. Koo, A. Kaczmarek, C. Xiao, J. Gao, X. Luo, Q. Niu, Y. Sun, B. Yan, L. Zhao, and A. W. Tsen, Giant c-axis nonlinear anomalous hall effect in td-mote2 and wte2, Nature Communications 12, 2049 (2021).

[28] M.-W. Hu, Z.-Y. Fang, H.-J. Duan, M. Yang, M.-X. Deng, and R.-Q. Wang, Modulation of chiral anomaly and bilinear magnetoconductivity in weyl semimetals by impurity resonance states, Phys. Rev. B 109, 155154 (2024).

[29] D.-F. Shao, S.-H. Zhang, G. Gurung, W. Yang, and E. Y. Tsymbal, Nonlinear anomalous hall effect for néel vector detection, Phys. Rev. Lett. 124, 067203 (2020).

[30] R. Chen, H.-P. Sun, M. Gu, C.-B. Hua, Q. Liu, H.-Z. Lu, and X. C. Xie, Layer hall effect induced by hidden berry curvature in antiferromagnetic insulators, National Science Review 11, nwac140 (2022).

[31] D. Zhang, M. Shi, T. Zhu, D. Xing, H. Zhang, and J. Wang, Topological axion states in the magnetic insulator mnbi$_2$te$_4$ with the quantized magnetoelectric effect, Phys. Rev. Lett. 122, 206401 (2019).

[32] R.-X. Zhang, F. Wu, and S. Das Sarma, Möbius insulator and higher-order topology in mnbi$_{2n}$te$_{3n+1}$, Phys. Rev. Lett. 124, 136407 (2020).

[33] H. Li, H. Jiang, C.-Z. Chen, and X. C. Xie, Critical behavior and universal signature of an axion insulator state, Phys. Rev. Lett. 126, 156601 (2021).

[34] W.-B. Dai, H. Li, D.-H. Xu, C.-Z. Chen, and X. C. Xie, Quantum anomalous layer hall effect in the topological magnet mnbi$_2$te$_4$, Phys. Rev. B 106, 245425 (2022).

[35] X.-X. Yi, C.-B. Hua, R. Chen, and B. Zhou, Disorder-enhanced layer hall effect in a magnetic sandwich heterostructure, Phys. Rev. B 109, 115301 (2024).

[36] A. Gao, Y.-F. Liu, C. Hu, J.-X. Qiu, C. Tzschaschel, B. Ghosh, S.-C. Ho, D. Bérubé, R. Chen, H. Sun, Z. Zhang, X.-Y. Zhang, Y.-X. Wang, N. Wang, Z. Huang, C. Felser, A. Agarwal, T. Ding, H.-J. Tien, A. Akey, J. Gardener, B. Singh, K. Watanabe, T. Taniguchi, K. S. Burch, D. C. Bell, B. B. Zhou, W. Gao, H.-Z. Lu, A. Bansil, H. Lin, T.-R. Chang, L. Fu, Q. Ma, N. Ni, and S.-Y. Xu, Layer hall effect in a 2d topological axion antiferromagnet, Nature 595, 521 (2021).

[37] Y. Feng, Y. Dai, B. Huang, L. Kou, and Y. Ma, Layer hall effect in multiferroic two-dimensional materials, Nano Letters 23, 5367 (2023).

[38] B. Chen, X. Liu, Y. Li, H. Tay, T. Taniguchi, K. Watanabe, M. H. W. Chan, J. Yan, F. Song, R. Cheng, and C.-Z. Chang, Even–odd layer-dependent exchange bias effect in mnbi2te4 chern insulator devices, Nano Letters 24, 8320 (2024).

[39] L. L. Tao, Q. Zhang, H. Li, H. J. Zhao, X. Wang, B. Song, E. Y. Tsymbal, and L. Bellaiche, Layer hall detection of the néel vector in centrosymmetric magnetoelectric antiferromagnets, Phys. Rev. Lett. 133, 096803 (2024).

[40] X. Wang, L. Bai, W. Feng, and Y. Yao, Layer nernst and thermal hall effects in two-dimensional antiferromagnets, Phys. Rev. B 111, 104405 (2025).

[41] S. Lai, H. Liu, Z. Zhang, J. Zhao, X. Feng, N. Wang, C. Tang, Y. Liu, K. S. Novoselov, S. A. Yang, and W.-b. Gao, Third-order nonlinear hall effect induced by the berry-connection polarizability tensor, Nature Nanotechnology 16, 869 (2021).

[42] J. P. Provost and G. Vallee, Riemannian structure on manifolds of quantum states, Communications in Mathematical Physics 76, 289 (1980).

[43] Y. Wang, Z. Zhang, Z.-G. Zhu, and G. Su, Intrinsic nonlinear ohmic current, Phys. Rev. B 109, 085419 (2024).

[44] N. Wang, D. Kaplan, Z. Zhang, T. Holder, N. Cao, A. Wang, X. Zhou, F. Zhou, Z. Jiang, C. Zhang, S. Ru, H. Cai, K. Watanabe, T. Taniguchi, B. Yan, and W. Gao, Quantum-metric-induced nonlinear transport in a topological antiferromagnet, Nature 621, 487 (2023).

[45] A. Gao, Y.-F. Liu, J.-X. Qiu, B. Ghosh, T. V. Trevisan, Y. Onishi, C. Hu, T. Qian, H.-J. Tien, S.-W. Chen, M. Huang, D. Bérubé, H. Li, C. Tzschaschel, T. Dinh, Z. Sun, S.-C. Ho, S.-W. Lien, B. Singh, K. Watanabe, T. Taniguchi, D. C. Bell, H. Lin, T.-R. Chang, C. R. Du, A. Bansil, L. Fu, N. Ni, P. P. Orth, Q. Ma, and S.-Y. Xu, Quantum metric nonlinear hall effect in a topological antiferromagnetic heterostructure, Science 381, 181 (2023).

[46] X. Zhang, Q. Liu, J.-W. Luo, A. J. Freeman, and A. Zunger, Hidden spin polarization in inversion-symmetric bulk crystals, Nature Physics 10, 387 (2014).

[47] S. Beaulieu, J. Schusser, S. Dong, M. Schüler, T. Pincelli, M. Dendzik, J. Maklar, A. Neef, H. Ebert, K. Hricovini, M. Wolf, J. Braun, L. Rettig, J. Minár, and R. Ernstorfer, Revealing hidden orbital pseudospin texture with time-reversal dichroism in photoelectron angular distributions, Phys. Rev. Lett. 125, 216404 (2020).

[48] E. Razzoli, T. Jaouen, M.-L. Mottas, B. Hildebrand, G. Monney, A. Pisoni, S. Muff, M. Fanciulli, N. C. Plumb, V. A. Rogalev, V. N. Strocov, J. Mesot, M. Shi, J. H. Dil, H. Beck, and P. Aebi, Selective probing of hidden spin-polarized states in inversion-symmetric bulk mos$_2$, Phys. Rev. Lett. 118, 086402 (2017).

[49] S. Cho, J.-H. Park, J. Hong, J. Jung, B. S. Kim, G. Han,

W. Kyung, Y. Kim, S.-K. Mo, J. D. Denlinger, J. H. Shim, J. H. Han, C. Kim, and S. R. Park, Experimental observation of hidden berry curvature in inversion-symmetric bulk $2h-$wse$_2$, Phys. Rev. Lett. **121**, 186401 (2018).

[50] W. Chen, M. Gu, J. Li, P. Wang, and Q. Liu, Role of hidden spin polarization in nonreciprocal transport of antiferromagnets, Phys. Rev. Lett. **129**, 276601 (2022).

[51] T.-R. Qin, Z.-H. Chen, T.-X. Liu, F.-Y. Chen, H.-J. Duan, M.-X. Deng, and R.-Q. Wang, Quantum hall effect in topological dirac semimetals modulated by the lifshitz transition of the fermi arc surface states, Phys. Rev. B **109**, 125111 (2024).

[52] Z.-X. Kong, Z.-Z. Xiong, W.-J. Wang, H.-J. Duan, M. Yang, M.-X. Deng, and R.-Q. Wang, Photon-assisted extrinsic weyl orbits and three-dimensional quantum hall effect in surface-doped topological dirac semimetals, Phys. Rev. B **110**, 075136 (2024).

[53] D. Kaplan, T. Holder, and B. Yan, Unification of nonlinear anomalous hall effect and nonreciprocal magnetoresistance in metals by the quantum geometry, Phys. Rev. Lett. **132**, 026301 (2024).

[54] J.-Y. Ba, Y.-M. Wang, H.-J. Duan, M.-X. Deng, and R.-Q. Wang, Nonlinear planar hall effect induced by interband transitions: Application to surface states of topo-

[55] logical insulators, Phys. Rev. B **108**, L241104 (2023).

[55] M. Kolodrubetz, V. Gritsev, and A. Polkovnikov, Classifying and measuring geometry of a quantum ground state manifold, Phys. Rev. B **88**, 064304 (2013).

[56] J. Wang, B. Lian, X.-L. Qi, and S.-C. Zhang, Quantized topological magnetoelectric effect of the zero-plateau quantum anomalous hall state, Phys. Rev. B **92**, 081107 (2015).

[57] H. Xu, H. Wang, J. Zhou, and J. Li, Pure spin photocurrent in non-centrosymmetric crystals: bulk spin photovoltaic effect, Nature Communications **12**, 4330 (2021).

[58] X. Mu, Q. Xue, Y. Sun, and J. Zhou, Magnetic proximity enabled bulk photovoltaic effects in van der waals heterostructures, Phys. Rev. Res. **5**, 013001 (2023).

[59] K. F. Mak, C. H. Lui, J. Shan, and T. F. Heinz, Observation of an electric-field-induced band gap in bilayer graphene by infrared spectroscopy, Phys. Rev. Lett. **102**, 256405 (2009).

[60] X.-G. Ye, H. Liu, P.-F. Zhu, W.-Z. Xu, S. A. Yang, N. Shang, K. Liu, and Z.-M. Liao, Control over berry curvature dipole with electric field in wte$_2$, Phys. Rev. Lett. **130**, 016301 (2023).

[61] R. Mei, D. Kaplan, B. Yan, C.-Z. Chang, and C.-X. Liu, Electrical control of intrinsic nonlinear hall effect in antiferromagnetic topological insulator sandwiches, Phys. Rev. B **110**, 165401 (2024).